Published in final edited form as:
Biochemistry. 2008 September 16; 47(37): 9900–9910. doi:10.1021/bi800828u.

Amylin Proprotein Processing Generates Progressively More Amyloidogenic Peptides that Initially Sample the Helical State†

Isaac T. Yonemoto[‡], **Gerard J. A. Kroon**[§], **H. Jane Dyson**[§], **William E. Balch**[||], and **Jeffery W. Kelly**[‡,*]

‡ *Department of Chemistry, The Skaggs Institute of Chemical Biology, The Scripps Research Institute, 10550 North Torrey Pines Road, La Jolla California 92037*

§ *Department of Molecular Biology, The Scripps Research Institute, 10550 North Torrey Pines Road, La Jolla California 92037*

|| *Department of Cell Biology, Institute for Childhood and Neglected Diseases, The Scripps Research Institute, 10550 North Torrey Pines Road, La Jolla California 92037*

Abstract

Human amylin, or islet amyloid polypeptide, is a peptide co-secreted with insulin by the beta cells of the pancreatic islets of Langerhans. The 37-residue, C-terminally amidated human amylin peptide derives from a proprotein that undergoes disulfide bond formation in the endoplasmic reticulum and is then subjected to four enzymatic processing events in the immature secretory granule. Human amylin forms both intracellular and extracellular amyloid deposits in the pancreas of most Type II diabetic subjects, likely reflecting compromised secretory cell function. In addition, amylin processing intermediates, postulated to initiate intracellular amyloidogenesis, have been reported as components of intracellular amyloid in beta cells. We investigated the amyloidogenicity of amylin and its processing intermediates *in vitro*. Chaotrope-denatured amylin and amylin processing intermediates were subjected to size exclusion chromatography, affording high concentrations of monomeric peptides. NMR studies reveal that human amylin samples helical conformations. Under conditions mimicking the immature secretory granule (37°C, pH 6), amylin forms amyloid aggregates more rapidly than its processing intermediates, and more rapidly than its reduced counterparts. Our studies also show that the amyloidogenicity of amylin and its processing intermediates is negatively correlated with net charge and charge at the C-terminus. Although our conditions may not precisely reflect the environment of amyloidogenesis *in vivo*, the lower amyloidogenicity of the processing intermediates relative to amylin suggests their presence in intracellular amyloid deposits in the increasingly stressed beta cells of diabetic subjects may be a consequence of general defects in protein homeostasis control known to occur in diabetes.

In type II diabetes, an increasing demand for insulin places a substantial stress on the protein secretion system of the beta cells of the islets of Langerhans, which results in cellular dysfunction and, eventually, beta cell death. As the population of beta cells continues to diminish, the stress on the remaining cells increases as they struggle to produce the insulin

†We thank the NIH (DK46335 and AG18917), The Skaggs Institute of Chemical Biology, and the Lita Annenberg Hazen Foundation for financial support.

*Corresponding author: jkelly@scripps.edu, phone: +1-858-784-9880, fax: +1-858-784-9610.

SUPPORTING INFORMATION AVAILABLE

Representative analytical ultracentrifugation data; NMR spectra, NMR resonance assignments and a table of resonances; as well as representative amyloidogenesis time courses are included. This material is available free of charge via the Internet at http://pubs.acs.org.

necessary to mount a proper host homeostatic response. This feedback loop is thought to be responsible for the progressive nature of type II diabetes (1).

Cross-β-sheet amyloid deposits are generally observed in the islets of Langerhans of type II diabetic subjects (2) and their presence correlates with the loss of beta cells (3). Whether amyloidogenesis causes, exacerbates, or results from beta cell dysfunction in humans are key unanswered questions being intensely investigated (2–5). The primary component of the amyloid deposits is amylin or islet amyloid polypeptide (IAPP), a peptide that is co-secreted with insulin by islet beta cells (3). Human amylin is a highly amyloidogenic peptide based on *in vitro* experiments, and amylin amyloidogenicity in organismal diabetes models correlates with beta cell death, although to date, a direct cause and effect relationship has been difficult to establish (2,6–8).

Although it is highly amyloidogenic *in vitro*, human amylin generally does not form amyloid deposits in healthy humans for reasons that are still being investigated. This is particularly interesting because the secretory granules exhibit very high concentration of peptides. Estimates of amylin concentration in the secretory granule range from ≤100 μM (based on a < 1:50 ratio with insulin (9,10) to 4 mM (11), and values in between (12). In addition to extracellular deposition, amylin amyloid has also been observed within the beta cells of type II diabetic subjects and in murine models (13–15). Proamylin processing intermediates comprise a portion of these intracellular deposits, suggesting that amylin misprocessing may trigger amyloid deposition (15).

In normally functioning beta cells, the 37-residue, C-terminally amidated amylin peptide derives from a 69-residue peptide, proamylin, that is endoproteolytically processed at the C-terminus of dibasic residue pairs (Lys12′, Arg13′) and (Lys52′, Arg53′), predominantly by the prohormone convertases PC 2 and PC 1/3, respectively (Scheme 1A), although both enzymes are believed to be capable of cleaving the other site, as well as a third site at the pair (Lys60′, Arg61′), albeit at a lower efficiencies (16–18). Endoproteolysis generates new N- and C-termini, the latter (Arg53′) is further processed by carboxypeptidase E (CPE), which removes the dibasic PC 1/3 recognition motif (KR) (19). The resulting peptide, containing an extra C-terminal glycine residue (Gly38), is referred to as amylin free acid. The peptidyl amidating monooxygenase (PAM) complex ablates the $C_\alpha H_2COOH$ substructure of the C-terminal Gly38 as a glyoxylate in the last processing step, affording amylin, which has an amide functional group at the new C-terminus (Tyr37). The proteolytic modifications are performed by the same enzymes which process proinsulin and are believed to occur in the acidified, immature secretory granule (20). In addition to these proteolytic modifications, native amylin also has a disulfide bond between Cys2 and Cys7, presumably formed in the oxidizing environment of endoplasmic reticulum, possibly via an enzyme-mediated reaction, and carried through in the oxidized state throughout the aforementioned processing steps.

A buildup in the concentration of one or more of the proamylin processing intermediates displayed in Scheme 1B has been implicated in amyloidogenesis and in beta cell death (15, 21). To understand their aggregation propensity, we synthesized, purified, and monomerized the amylin processing intermediates and evaluated their relative amyloidogenesis at pH 6, 37 °C. Biophysical studies on monomerized amylin reveal that the majority of the peptide samples helical conformational states. The transformation of amylin from a soluble peptide to an amyloid cross-β-sheet structure is extremely rapid. The amyloidogenesis of amylin free acid and reduced amylin (dithiol) is significantly slower and seems to occur in an energetically downhill fashion at high concentrations. Aggregation of the remaining amylin processing intermediates is slower yet, with their relative rates of amyloidogenesis correlating negatively with net charge and charge flanking the putative amyloid core. Thus processing of proamylin generates progressively more amyloidogenic peptides, with the final product, amylin, being

the most amyloidogenic under conditions (pH 6, 37°C) envisioned to simulate the immature secretory granule, although we cannot be sure that these conditions mimic the environment of amylin amyloidogenesis *in vivo*.

EXPERIMENTAL PROCEDURES

Materials

Sodium phosphate, guanidinium chloride (GdnHCl), urea, EDTA (electrophoresis grade); sodium azide (Biotech research grade); 2-propanol and acetonitrile (HPLC grade) were obtained from Fisher Scientific (Fair Lawn, NJ). 3-(trimethyl silyl) propane sulfonic acid (DSS) was obtained from Cambridge Isotope Labs (Andover, MA). Tris (ultrapure grade) was obtained from Invitrogen (Carlsbad, CA). MES and TCEP were obtained from Aldrich (Milwaukee, WI). Boc- and Fmoc-protected amino acids were obtained from Novagen (La Jolla, CA). Practical grade GdnHCl was obtained from MP Biochemicals (Solon, OH) and recrystallized by adding a minimal amount of water, boiling, and adding an equal volume of 2-propanol, cooling at 4 °C and redissolving in water with the addition of activated charcoal to decolorize the solution. Buffers were prepared in deionized water ultrafiltered using a Quantum EX apparatus from Millipore (Billerica, MA); to ensure reproducibility all analytical buffers were created from 20x stocks except where noted. Thioflavin T was obtained from Sigma-Aldrich (Milwaukee, WI) and was recrystallized as described in the literature (22) prior to generation of a 100 mM stock in a 10 mM phosphate, pH 6.0 buffer containing 100 mM NaCl.

Human Amylin Synthesis and Purification

Lyophilized amylin free acid was obtained from SynPep (Dublin, CA) and was stored at −80 °C. The purity (> 95%) was confirmed by RP-HPLC on a C18 column. ESI-MS confirmed the correct mass and analytical RP-HPLC retention shifts following treatment by dithiothreitol (DTT) and 2-mercaptoethanol (BME) confirmed that the disulfide bond was correctly formed. Reduced amylin free acid was prepared from the oxidized peptide by incubation at 10 mg/mL in a 10 mM phosphate, pH 6.0 solution containing 6 M GdnHCl, 100 mM NaCl, and 2% (v/v) 2-mercaptoethanol, and was purified by RP-HPLC prior to lyophilization and use. Amylin was synthesized following the protocol of Abedini and Raleigh (23), with the following modifications: double-coupling was performed only when coupling non pseudoproline residues succeeding the first pseudoproline dipeptide; relyophilization prior to HPLC was performed 6 times from 30% acetonitrile (ACN), 0.01% trifluoroacetic acid (TFA) (v/v); after relyophilization, amylin was precipitated from nonpeptide residual products in 95% ACN, 0.01% TFA (v/v) and purified by preparative HPLC over two cycles (Vydac Z18TPN022, Phenomenex Jupiter 4u Proteo 90A), affording the reduced peptide; oxidation was performed in 7.2 M GdnHCl, 10 mM Tris, pH 8.5, by titrating by color in the same solution with 1% $K_2Fe(CN)_6$ (w/v), followed by incubation at 4°C overnight. A typical 100 μM preparative synthesis yielded 20 mg dry mass of purified, oxidized product. Amylin+NT (1′–50′, amide) was produced following the above protocol based on an updated synthesis (24). Double-coupling was only performed on beta-branched residues and residues following beta-branched residues after the first pseudoproline residue, and synthesis was terminated at the first cysteine residue (2–37, amide) but otherwise the synthesis was identical to that of amylin. A second peptide (1′–14′-Mpa-Leu/His8′-DNP) was synthesized using BOC chemistry, affording a yellow peptide. This peptide was then coupled to the (2–37) peptide under denaturing native chemical ligation conditions, 10 mM phosphate, 7.2 M GdnHCl, 1% (v/v) thiophenol, pH 7.4., and repurified by C18 HPLC chromatography. Amylin (oxidized disulfide and reduced dithiol); and amylin free acid (oxidized disulfide and reduced dithiol) were stored lyophilized at −80 °C.

Recombinant Preparation of Human Amylin Processing Intermediates

Amylin+KR (14′–52′), amylin+CT (14′–69′) and proamylin (1′–69′) were expressed using a common protocol. These peptides were generated as fusions to a codon-optimized BCL-XL-1/2 protein in modified pBAD vectors (details to be published elsewhere and provided upon request in the interim period). The construct and inserts were generated using a combination of assembly PCR and standard molecular biology techniques. BL-21 (DE3) E. Coli cells were transformed with the vector and grown in pH 7.4 LB medium and harvested 2 h after induction with 0.1% w/v arabinose at OD 600 = 0.8, frozen overnight and subjected to two cycles of resuspension, sonication and pelleting in pH 8.0 50 mM Tris, 100 mM NaCl, 0.1% (v/v) Triton-X 100, 50 mM EDTA, 0.02% (w/v) sodium azide, 0.05% (w/v) DNAse A, two cycles in the same buffer without DNAse or Triton-X 100, and two cycles in pH 5.0 50 mM Tris, 50 mM MES, 100 mM NaCl, 0.02% (w/v) sodium azide. The remaining pellet was then resuspended in pH 8.5 50 mM Tris, 7.2 M GdnHCl (practical grade), 1 mM TCEP, and stirred for one week. The solubilized pellet was then centrifuged twice at 50,000 g for 1 h to clarify the solution, and loaded onto a TALON cobalt IMAC column.

The column was washed using 50 mM Tris (pH 8.5), 7.2 M GdnHCl, and the peptide was eluted using 50 mM Tris (pH 5.0), 50 mM MES, 7.2 M GdnHCl. The peptides were subjected to purification by RP-HPLC using a C4 (Vydac 214TP1022) column. The lyophilized peptides were then resolubilized at 20 mg/mL in 7.2 M GdnHCl, 0.1 M excess HCl, and subjected to cleavage using 1:4 dilution of a 20 mg/mL solution of cyanogen bromide in the same buffer and incubated at RT overnight in the dark. All amylin intermediates were stored lyophilized at −80 °C.

General Pretreatment to Remove Aggregates and Monomerize Human Amylin and its Processing Intermediates

Prior to use, 1~6 mg of the lyophilized peptide, depending on the desired final concentration, was dissolved in 650 μL of 10 mM phosphate buffer (pH 6.0) containing 7.5 M GdnHCl and 100 mM NaCl. For reduced amylin, 6 μL of BME was added to ensure disulfide reduction. The denatured amylin solution was sonicated for 5 min to ensure maximal dissolution. This solution was filtered through a 0.22 μm syringe-driven filter and loaded onto a Superdex 30 column pre-equilibrated in a filtered, autoclaved 10 mM phosphate buffer (pH 6.0) containing 100 mM NaCl. For kinetic studies, the conductivity of the solution at 4 °C was 13 ± 1 mS/cm as determined by an inline conductivity meter (Amersham Pharmacia). Amylin or its processing intermediates were eluted at 4 °C and kept on ice for immediate usage.

NMR Spectroscopy of Human Amylin

Amylin free acid solution (400 μL of ~250 μM solution), monomerized as described directly above, was added to 100 μL of 10 mM phosphate buffer (uncorrected pH/D 6.0) containing 50% D_2O, 0.02% NaN_3 (w/v) and 0.05% (w/v) DSS. This solution was transferred into a NMR tube (Kontes) which had been cleaned thoroughly with detergent and boiled for 20 minutes in 1 M NaOH and 1 M HCl successively, rinsed in buffer, and dried prior to loading sample. This was placed on ice until transfer into an Avance 500 MHz NMR spectrometer (Bruker) with a 5 mm TXI probe. The sample temperature was preset to 278 K. DQF-COSY, TOCSY, and NOESY experiments (100, 150, and 300 ms mixing time) were performed sequentially with 1D experiments performed between each experiment to ensure that aggregation had not occurred. For spectroscopic experiments, reduced amylin was prepared after purging FPLC buffers with argon and pre-treating the size exclusion column with a blank run consisting of guanidine and DTT. Amylin (oxidized disulfide and reduced dithiol) aggregated in the spectrometer within 10 hours at NMR concentrations, and was subjected to DQF-COSY and 150 ms mixing time NOESY experiments only, with fresh preparations performed between each spectroscopic experiment.

CD Spectroscopy of Human Amylin

Amylin free acid was monomerized as described above and its concentration was determined by UV and adjusted to 250 or 200 μM (OD 276 = 1660 M AU^{-1} cm^{-1}), depending on yield. 80 or 100 μL of this material was added to 320 or 300 μL, respectively, of 10 mM phosphate buffer (pH 6.0) containing 100 mM NaCl and adjusted concentrations of denaturant (guanidine or urea for denaturation curves) and lightly agitated by hand to ensure proper mixing, resulting in a final amylin concentration of 50 μM. This solution was loaded into a 2 mm quartz cell (Hellma QC) and CD spectra were obtained using a CD spectropolarimeter (AVIV 202SF) and corrected with a matching background.

At each denaturation point, three spectra were taken between 250 nm and 215 nm wavelengths at 0.5 nm increments with 1 s integration times and averaged, then the chaotrope concentration was measured using refractometry. Each denaturation scan was performed three times with additional data collected in the transition and post-transition regions.

Electron Microscopy of Human Amylin and its Processing Intermediates

Amylin was monomerized as described above, except with 0.02% (w/v) NaN_3 in elution buffers, and its concentration was determined by UV and adjusted to 100 μM. A freshly prepared solution was seeded (10%) with a solution of sonicated, aggregated amylin or amylin processing intermediate fibrils composed of the same sequence of the peptide in solution, and left to incubate overnight. The aggregated solution was desalted by pelleting, decanting, and resuspension in deionized water. 10 μL of aggregate solution were dropped onto an EM grid, incubated for 1 min, and wicked off. 10 μL of freshly prepared solution of 2% (w/v) uranyl acetate, 50% EtOH were then dropped on top of the adsorbed fibrils, incubated for 1 min, and wicked off. Grids were air-dried overnight and then observed in a Philips CM-100 electron microscope at 80 kV acceleration energy. Micrographs were taken using Kodak S0162 film.

ThT Fluorescence-Monitored Amyloidogenesis Kinetics of Human Amylin and its Processing Intermediates

Amylin amyloidogenesis was monitored by the amyloid binding dye, thioflavin T. Amylin was monomerized as described above, except with 0.02% (w/v) NaN_3 in elution buffers, and its concentration was adjusted by UV to 111% of the desired experimental concentration. Amylin solution (360 μL) was added on ice to a 10 mm quartz cell (HELLMA QC) containing 40 μL of 1 mM thioflavin T solution, pH 6.0. The cuvette was then lowered into a spectrofluorimeter (AVIV ATF 105) pre-equilibrated at 37 °C. Fluorimetry readings were taken every 30, 60 or 120 seconds with 1s averaging times. Measurements were taken around an excitation wavelength of 440 nm and an emission wavelength of 485 nm with 5 nm bandwidths. Readings were normalized against the autofluorescence of a solution containing 1 mM ThT incubated at 25 °C. Cuvettes were rinsed with 0.5 M NaOH, and incubated for 3 h (minimum) in Alconox detergent followed by incubation for 3 h (minimum) in conc. nitric acid. Kinetic measurements were repeated 5 times at each condition (oxidized amylin and amylin free acid) or 4 times at each condition (reduced amylin and amylin free acid, processing intermediates). Fluorescence intensity was replotted as fraction complete, renormalizing based on the highest and lowest set of 10 sequential points. t_{50} was calculated by fitting the curve to a stretched exponential and error for each individual experiment was calculated based on error analysis of the asymptotic standard errors for each term.

RESULTS and DISCUSSION

Aqueous chaotrope pretreatment followed by gel filtration affords monomeric human amylin

The aggregation state of peptides in lyophilate is generally not well characterized. For amylin and its processing intermediates, the elimination of amyloid fibrils and oligomeric seeds, which would hasten aggregation, was a general concern in all experiments. Historically, removal of aggregates has been achieved by dilution of amylin stocks prepared in organic solvents. The solvents utilized include trifluoroethanol (TFE) (25), hexafluoroisopropanol (HFIP) (24,26–37), and dimethylsulfoxide (DMSO) (26,38), which disassemble beta-sheet aggregates of amylin by favoring alpha helical peptide conformations or by eliminating the hydrophobic effect critical for the stability of the amyloid state, or both. The preparation of amylin by dissolution in HFIP followed by lyophilization and reconstitution in deionized water has been previously reported (17,36). However, this preparation resulted in rapid aggregation when reconstituted in salt-containing buffers and the aggregation state of this preparation was not well defined (17,36).

We avoided solvent pretreatment approaches because the denaturing solvents persist after aqueous dilution; because the fluorinated solvents are known to accelerate amylin amyloidogenesis, despite stabilizing helical conformations (29); and because of the ill-characterized aggregation state in lyophilate. For all experiments in this study, the removal of aggregates was achieved by chaotrope denaturation of the lyophilized amylin peptide or processing intermediate, followed by size exclusion chromatography into the desired buffer. This approach for monomerization has been used concurrently for other aggregation-prone peptides in our laboratory and by others, and appears to be generally efficacious (39,40).

The conductivity of the fractions containing amylin or amylin processing intermediates matched the conductivity of the elution buffer (Figure 1), confirming the lack of denaturant in these fractions. Both the elution volume and analytical ultracentrifugation analysis of a representative preparation of amylin free acid (see Supporting Information) suggest a hydrodynamic radius of a globular protein with a mass of 7 kDa, consistent with that of a monomeric, partially unfolded peptide like amylin, although trace repopulation of small oligomers cannot be ruled out from these data alone.

NMR spectroscopy of human amylin reveals that it samples helical conformations

In order to ascertain the structures of human amylin in a biologically relevant buffer (pH 6), several 2D spectra were obtained, as described in the Experimental Procedures section, over the course of 5 days at 278 K. The 1D NMR spectra of amylin recorded after each 2D experiment did not change appreciably, confirming that aggregation did not occur at this temperature on this timescale. Spectra and resonance assignments for human amylin free acid obtained in these studies are provided in the Supporting Information. Resonance assignments were obtained using amylin free acid because it is less aggregation prone than amylin. However, analogous resonances were found in the spectra of amylin.

Analysis of the NMR spectra of human amylin (10 mM phosphate buffer, pH 6.0, 100 mM NaCl) revealed that the N-terminus preferentially populates backbone dihedrals in the alpha region, indicative of helical conformations, with no detectable beta strand or sheet structure, in contrast to previous models (5,41). Unambiguous long-range side-chain to side-chain NOE resonances were not observed in soluble human amylin, suggesting the peptide does not adopt a unique 3D structure or fold. Amide proton chemical shift deviations (Figure 2A) in human amylin are similar to those found in the homologous rat amylin by the Miranker group – consistent with an N-terminus (residues 1–20) with a modest helical propensity and a C-terminus that is less structured (residues 21–37) (42). However, Cα proton chemical shift

deviations (Figure 2B) suggest that human amylin shows greater helical propensity than rat amylin across the entire peptide, markedly so in the C-terminal half of human amylin. We also observe strong (i, i+1) amide-amide NOEs across the entire sequence of human amylin; indicative of a peptide backbone that samples alpha-helical backbone dihedrals (Figure 2C). However, no significant (i, i+3) alpha-amide or (i, i+4) alpha-amide NOEs were observed, which if observed, would be diagnostic of a well-folded helical conformation. Hence, human amylin adopts a conformation similar to, but seemingly more structured than that found in the murine homolog and amylin's nearest paralogous relative, calcitonin (43,44). The increased helical propensity of the C-terminus of human amylin relative to rat amylin can be rationalized by the presence of three proline residues in the latter, which would act as helix breakers. Interestingly, the presence of these prolines in the rat peptide is also thought to abrogate its amyloidogenicity (8,30). It is possible that the higher amyloidogenicity of the human peptide necessitates the observed enhanced helicity in its C-terminus to protect against aberrant aggregation in the secretory pathway.

Our NMR data also reveal that the disulfide bond at the N-terminus of human amylin imparts an unusual structure to this region. Unlike almost all the other residues in amylin, Thr4 and Ala5 show no amide-amide NOE. Instead, a Thr4 - Ala8 NOE is observed (Figure 2D). There are strong sequential amide NOEs between residues 6–8 and a strong NOE between the amide protons of residue 4 and residue 5. Together, these data suggest that the disulfide bond orients the amide bonds of residues 4 and 5 in a direction opposite to the alignment established by the helix sampled by the remainder of the peptide; residues 6 through 8 are twisted to accommodate this change in direction. This unusual conformation likely results in a net destabilization of the helical conformational ensemble in this region.

A previous NMR study reported a helical structure for human and rat amylins, with spectra being recorded in a solution containing 25% (v/v) HFIP–a helix inducing solvent. In that study, two helical segments were observed: one from residues 7–17 and another from residues 23–29 (25). Our NMR data, collected in the absence of organic solvents, are more consistent with a peptide sampling helical conformations extending over the majority of human amylin, except in the N-terminal disulfide region. While increasing beta-structure was observed as the HFIP concentration was decreased (25), we observe no evidence of β-structure in purely aqueous buffers at pH 6.

The helical conformations that human amylin samples can be denatured using chaotropes

Far-UV CD spectra of amylin free acid in buffer with and without 4 M guanidine differ significantly, suggesting that the population of helical states being sampled is high enough to be altered by denaturant (Figure 3A). Previous attempts at amylin denaturation have reported unusual denaturation profiles, with dichroic extrema observed at intermediate denaturant concentrations (45). In contrast, we observed a smooth increase in mean residue ellipticity (MRE) with increasing denaturant concentration (Figure 3B, 3C). Moreover, the transitions are modestly cooperative, further supporting the idea that the population sampling helical conformations is low, but finite (Figure 3B, 3C). Thermal denaturation was attempted (data not shown) but visible aggregates formed inside the cuvette, likely triggered by the incubation of the peptide solution at elevated temperatures for extended periods.

Human amylin and its processing intermediates exhibit similar fibrillar morphology

Human amylin, amylin free acid, and their processing intermediates: amylin+KR, amylin+NT, amylin+CT, as well as proamylin (see Scheme 1B for sequences) all generated aggregates exhibiting a fibrillar structure when examined by electron microscopy (Figure 4). These fibrils were all generated in the quiescent state overnight at 37 °C. Amylin and its processing intermediates were seeded with fibrils composed of the respective peptides also generated

overnight in the quiescent state, except for proamylin, which was seeded with proamylin fibrils generated by rotary agitation. The fibrils all exhibited a similar diameter and a helical pitch, and formed higher order assemblies of twisted fibrils. The similar morphologies of the fibrils suggest a common structure, although subtle conformational differences cannot be ruled out by examining the fibrils using electron microscopy alone. Even if the structures are nearly identical, their mechanisms of assembly could be quite different.

Human amylin free acid transitions from concentration-dependent to concentration-invariant aggregation kinetics

Although the shape of individual kinetic traces for oxidized (intact disulfide) and reduced human amylin free acid suggest the assembly of these amyloids is not likely to be a singly nucleated polymerization process (Figure 5A and Supporting Information), we found that the concentration dependence of amyloidogenesis can be rationalized using this model. The data are consistent with the existence of a high-energy on-pathway oligomeric species or nucleus that is a prerequisite to fibril assembly. This is evident as velocity increases with concentration at low concentrations while converging toward a maximum velocity at high concentrations (Figure 5B). At these concentrations, amyloidogenesis becomes an energetically downhill process, with the rate limiting step being conversion of monomer to an amyloid competent species.

To explain this unusual phenomenon, we recall Powers and Powers' report that while traditional nucleated polymerizations exhibit a linear relationship between log(concentration) and log(t_{50}), this relationship can be lost at high concentration without a change in assembly mechanism or energies of association, including enthalpy of binding, and configurational and solvent expulsion entropies (46). Elevated concentrations will, however, alter the entropy of assembly, resulting in an overall decrease of the energetic penalty of monomer addition to oligomers. In particular, beyond a certain concentration (supercritical concentration, K_s), the enthalpic and solvent expulsion contributions can overcome the entropic penalty of oligomer assembly, resulting in downhill polymerization kinetics without a change in assembly mechanism. It appears that amylin free acid and reduced amylin free acid undergo a similar transition from concentration-dependent kinetics to concentration-invariant kinetics. Notably, this transition appears to occur across a supercritical concentration that is likely to be below the native concentration of amylin in the immature secretory granule (9–12).

Oxidized human amylin free acid aggregates more rapidly than reduced amylin free acid

The reduced form of amylin free acid aggregated slower than that of the oxidized form (Figure 5B, unfilled vs. filled circles, respectively). For amylin free acid, the data suggest that the kinetics are shifted by a similar velocity across all concentrations evaluated. If fibril dissociation rates are similar, then the difference in amyloidogenesis kinetics between the two forms is likely to be the result of a difference in the rate of prenuclear assembly. This suggests that the disulfide bond, while thought to generally protect the peptide from N-terminal proteolytic degradation, has the effect of destabilizing the soluble helical conformations relative to the amyloid competent beta sheet conformations. This may be due to the helix-destabilizing orientation of amide bonds in residues 3 and 4 (*vide supra*), which appear to be in opposition to the polarity established by the helix sampled by the remainder of the peptide.

Human amylin is more amyloidogenic than human amylin free acid

We hypothesized that amylin misprocessing, resulting from the failure of the PAM complex oxidation machinery to remove the glyoxylate, would result in the production of a more amyloidogenic peptide. Previous publications have not addressed the difference in amyloidogenicity between amylin free acid and amylin. We observed that amylin (filled

squares; Figure 5B) aggregates faster than amylin free acid in both oxidized (Figure 5B, filled circles) and reduced states (Figure 5B, open circles) over a broad range of concentrations.

A plot of t_{50} vs amylin concentration reveals that reduced amylin free acid and reduced amylin exhibit similar concentration dependent kinetic profiles (Figure 5B, open circles vs. open squares), although reduced amylin aggregates faster and reaches a limiting velocity at a lower concentration. Assuming a common assembly mechanism, reduced human amylin's supercritical concentration is decreased and the maximum velocity is increased relative to reduced human amylin free acid, suggesting that there is an increase in the rate of prenuclear assembly and also an increased enthalpy of assembly. Both of these trends are consistent with the elimination of a negative charge from the C-terminal carboxylate of amylin, believed to flank the amyloid core (40, Figure 6).

Human amylin exhibits a t_{50} vs concentration kinetic profile (Figure 5B, solid squares) dissimilar to that of oxidized and reduced human amylin free acid and dissimilar to that of reduced human amylin, all plotted in Figure 5B. We were unable assess the aggregation kinetics of human amylin at very high concentrations due to prohibitive quantities required relative to availability; however, in the range of concentrations tested, it does not appear that we reached the maximum velocity of amyloid assembly. Nonetheless, aggregation of human amylin with its disulfide bond intact becomes very fast at concentrations exceeding 100 μM. Although we cannot assume that the aggregation of human amylin is a downhill process either *in vitro* or *in vivo* (i.e. that we exceeded its supercritical concentration), the aggregation occurred more rapidly than for amylin free acid or reduced amylin. The dramatically different kinetic profile (Figure 5B) further suggests that oxidized human amylin may aggregate via a different mechanism than its processing intermediates.

Native human amylin is more amyloidogenic than its processing intermediates

In addition to studying the kinetics of oxidized and reduced amylin and amylin free acid discussed directly above, we evaluated the amyloid propensity of four other possible human amylin processing intermediates. These include proamylin and intermediates corresponding to a failure of the processing machinery required to produce human amylin from proamylin. Amylin+NT corresponds to human amylin with an extended N-terminus, which could arise from the failure of PC 2 endoproteolysis. Amylin+CT corresponds to human amylin with an extended C-terminus, which could arise from the failure of the PC 1/3 endoproteolysis. Amylin +KR corresponds to the human amylin produced as a result of a failure of carboxypeptidase E activity, and amylin free acid, evaluated above, corresponds to the peptide produced as a result of failure of PAM complex oxidation that removes the glyoxylate and affords the C-terminal amide of human amylin.

When compared to amylin, proamylin was less amyloidogenic at equal concentrations of 100 μM, as previously reported in the literature (47, Figure 5C). We further established that proamylin was the least amyloidogenic peptide in the processing pathway of amylin. Indeed, it did not exhibit amyloidogenesis in solution when left in a quiescent state over the course of 6 days. Beyond this time, aggregates were observed at the air-water interface where concentration due to evaporation was occurring. However, overnight agitation of proamylin in a rotary shaker (24 rpm) afforded aggregates which were competent to seed the quiescent amyloidogenesis of monomerized proamylin, as confirmed by EM (Figure 4E).

Unlike proamylin, the other human amylin processing intermediates all exhibited amyloidogenesis without seeding to varying degrees when subjected to quiescent aggregation at a concentration of 100 μM. Of these, amylin free acid was the most amyloidogenic, followed by amylin+NT, amylin+KR, and amylin+CT (Figure 5C) in that order. This trend can be explained biophysically by comparing the charge states of these peptides. In particular,

aggregation propensity correlates negatively with increasing charge after what would be the C-terminus (Tyr50′) of the core β-strand (core strand) in the amylin amyloid fibril (Figure 6), based on solid state NMR evidence (40). Since each strand is arranged with the side chains in an in-register fashion (40), the charges must also be in-register, rationalizing how the presence of these charges would be enthalpically destabilizing, rendering the overall hydrophobic burial process less energetically favorable or prohibitive. The aggregation propensities of the processing intermediates of amylin also seem to be negatively affected by the increasing net charge on the peptide as a whole (Figure 6). Both of these observations are in accordance with the general principle that charge reduces amyloidogenicity (48).

SUMMARY and PERSPECTIVE

We have developed an aggregate removal protocol that affords human amylin and human amylin processing intermediates as metastable monomers in the desired aqueous buffer–by chaotrope denaturation followed by gel filtration chromatography as a critical finishing step. Experimental evidence demonstrates that this is a reliable way of eliminating seeds, allowing for highly reproducible structural and kinetic aggregation studies to be accomplished *in vitro*.

Access to high concentrations of human amylin and its processing intermediates, afforded by the new monomerization protocol, enabled exploration of the concentration dependence of fibril assembly kinetics under conditions closer to those found in the secretory pathway of the islet beta cell (9–12). We report that all of the human amylin processing intermediates are less amyloidogenic at pH 6, 37 °C than oxidized, amidated amylin itself, consistent with previous reports that proamylin is much less amyloidogenic than amylin (47). The decreased amyloidogenicity of the amylin processing intermediates relative to amylin is rationalized by the increased net charge on the human amylin processing intermediates and the increased in register charges in the C-terminal extension sequences directly flanking the amylin amyloid core.

Progress along the human amylin processing pathway (Scheme 1) generates amylins of progressively increasing amyloidogenicity (Figure 5C). While misprocessing of amylin has been implicated as a causative factor in generating the intracellular amylin deposits found in type II diabetes models and in humans (13–15), the lowered amyloidogenicity of the processing intermediates observed under our conditions seems inconsistent with this hypothesis. However, it is possible that our *in vitro* conditions do not precisely mimic the environment of amyloidogenesis *in vivo*, to the extent that the differences would change the amyloidogenicity rankings of amylin and its processing intermediates that we observe *in vitro* (Figure 5C). For example, altered binding to secretory granule components believed to sequester amylin and preclude amyloidogenesis (9–12) may overcome the gross differences in amyloid propensity we observed.

It seems more likely to us that the discovery of amylin processing intermediates deposited as amyloid within beta cells reflects a general defect in protein homeostasis control known to occur in diabetes (49), rather than being a trigger of pathology (50). That the N- and C-terminal extensions present in the processing intermediates of human amylin have a protective effect against amyloidogenesis, further leads us to speculate that part of their function may be to prevent aggregation and amyloidogenesis in early stages of amylin biosynthesis and transport through the exocytic pathway. The highly amyloidogenic nature of human amylin is peculiar, suggesting that its amyloidogenicity may have something to do with its function or that residues required for some function in humans confer amyloidogenicity.

Supplementary Material

Refer to Web version on PubMed Central for supplementary material.

Abbreviations

BME
2-mercaptoethanol

CPE
carboxypeptidase E

DMSO
dimethyl sulfoxide

DQF-COSY
double quantum-filtered correlation spectroscopy

DSS
3-(trimethylsilyl) propane sulfonic acid

DTT
dithiothreitol

EDTA
ethylenediaminetetraacetate

ESI-MS
electrospray ionization mass spectrometry

FPLC
fast protein liquid chromatography

GdnHCl
guanidinium chloride

HFIP
1,1,1,3,3,3-hexafluoro 2-propanol

IAPP
islet amyloid polypeptide

IMAC
immobilized metal affinity chromatography

LB
Luria-Bertani broth

MES
morpholino ethane sulfonic acid

MRE
mean residue ellipticity

NMR
nuclear magnetic resonance

NOE
nuclear Overhauser effect

NOESY
nuclear Overhauser effect spectroscopy

PAM
peptidyl amino monooxygenase

PC
prohormone convertase

RP-HPLC
reverse-phase high performance liquid chromatography

TCEP
tris (carboxyethyl) phosphine

TFA
trifluoroacetic acid

TFE
trifluoroethanol

TOCSY
total correlation spectroscopy

Acknowledgements

We thank Johan Paulsson for assistance with the uranyl acetate staining protocol and for reading the manuscript, Colleen Fearns for careful editing of the manuscript, Malcolm Wood and Theresa Fassel for assistance in developing electron micrographs, Sarah Siegel for assistance with analytical ultracentrifugation, and Evan Powers for his expert advice on kinetics.

References

1. Marzban L, Park K, Verchere CB. Islet amyloid polypeptide and type 2 diabetes. Exp Gerontol 2003;38:347–351. [PubMed: 12670620]
2. Westermark P, Wernstedt C, Wilander E, Hayden DW, O'Brien TD, Johnson KH. Amyloid fibrils in human insulinoma and islets of Langerhans of the diabetic cat are derived from a neuropeptide-like protein also present in normal islet cells. Proc Natl Acad Sci U S A 1987;84:3881–3885. [PubMed: 3035556]
3. Westermark P, Wernstedt C, Wilander E, Sletten K. A novel peptide in the calcitonin gene related peptide family as an amyloid fibril protein in the endocrine pancreas. Biochem Biophys Res Commun 1986;140:827–831. [PubMed: 3535798]
4. Haataja L, Gurlo T, Huang CJ, Butler PC. Islet amyloid in type 2 diabetes, and the toxic oligomer hypothesis. Endocr Rev 2008;29:303–316. [PubMed: 18314421]
5. Jaikaran ET, Clark A. Islet amyloid and type 2 diabetes: from molecular misfolding to islet pathophysiology. Biochim Biophys Acta 2001;1537:179–203. [PubMed: 11731221]
6. Jordan K, Murtaugh MP, O'Brien TD, Westermark P, Betsholtz C, Johnson KH. Canine IAPP cDNA sequence provides important clues regarding diabetogenesis and amyloidogenesis in type 2 diabetes. Biochem Biophys Res Commun 1990;169:502–508. [PubMed: 2192709]
7. Matvyenko AV, Butler PC. β-Cell Deficit Due to Increased Apoptosis in the Human Islet Amyloid Polypeptide Transgenic (HIP) Rat Recapitulates the Metabolic Defects Present in Type 2 Diabetes. Diabetes 2006;55:2106–2114. [PubMed: 16804082]
8. Betsholtz C, Christmanson L, Engstrom U, Rorsman F, Svensson V, Johnson KH, Westermark P. Sequence divergence in a specific region of islet amyloid polypeptide (IAPP) explains differences in islet amyloid formation between species. FEBS Letters 1998;251:261–264.

9. Janciauskiene S, Eriksson S, Carelemalm E, Ahren B. B Cell Granule Peptides Affect Human Islet Amyloid Polypeptide (IAPP) Fibril Formation *in Vitro*. Biochem Biophys Res Commun 1997;236:580–585. [PubMed: 9245692]
10. Hutton JC. The Insulin Secretory Granule. Diabetologia 1989;32:271–281. [PubMed: 2526768]
11. Nishi M, Sanke T, Nagamatsu S, Bell GI, Steiner DF. Islet Amyloid Polypeptide. J Biol Chem 1990;265:4173–4176. [PubMed: 2407732]
12. Larson JL, Miranker AD. The Mechanism of Insulin Action of Islet Amyloid Polypeptide Fiber Formation. J Mol Biol 2004;335:221–231. [PubMed: 14659752]
13. de Koning EJ, Morris ER, Hofhuis FM, Posthuma G, Hopener JW, Morris JF, Capel PJ, Clark A, Verbeek JS. Intra- and extracellular amyloid fibrils are formed in cultured pancreatic islets of transgenic mice expressing human islet amyloid polypeptide. Proc Natl Acad Sci USA 1994;91:8467–8471. [PubMed: 8078905]
14. O'Brien TD, Butler AE, Roche PC, Johnson KH, Butler PC. Islet amyloid polypeptide in human insulinomas. Evidence for intracellular amyloidogenesis. Diabetes 1994;43:329–336. [PubMed: 8288058]
15. Paulsson JF, Andersson A, Westermark P, Westermark GT. Intracellular amyloid-like deposits contain unprocessed pro-islet amyloid polypeptide (proiapp) in beta cells of transgenic mice overexpressing the gene for human iapp and transplanted human islets. Diabetologia 2006;49:1237–1246. [PubMed: 16570161]
16. Marzban L, Trigo-Gonzalez G, Zhu X, Rhodes CJ, Halban PA, Steiner DF, Verchere CB. Role of beta-cell prohormone convertase (pc)1/3 in processing of pro-islet amyloid polypeptide. Diabetes 2004;53:141–148. [PubMed: 14693708]
17. Higham CE, Hull RL, Lawrie L, Shennan KI, Morris JF, Birch NP, Docherty K, Clark A. Processing of synthetic pro-islet amyloid polypeptide (proiapp) 'amylin' by recombinant prohormone convertase enzymes, pc2 and pc3, in vitro. Eur J Biochem 2000;267:4998–5004. [PubMed: 10931181]
18. Wang J, Xu J, Finnerty J, Furuta M, Steiner DF, Verchere CB. The Prohormone Convertase Enzyme 2 (PC2) Is Essential for Processing Pro-Islet Amyloid Polypeptide at the NH2-Terminal Cleavage Site. Diabetes 2001;50:534–539. [PubMed: 11246872]
19. Marzban L, Souchatkeva G, Verchere CB. Role of Carboxypeptidase E in Processing of Pro-Islet Amyloid Polypeptide in β-Cells. Endocrinology 2005;146:1808–1817. [PubMed: 15618358]
20. Orci L, Halban P, Perrelet A, Amherdt M, Ravazzola M, Anderson RG. pH-independent and -dependent cleavage of proinsulin in the same secretory vesicle. J Cell Biol 1994;126:1149–1156. [PubMed: 8063854]
21. Paulsson JF, Westermark GT. Aberrant processing of human proislet amyloid polypeptide results in increased amyloid formation. Diabetes 2005;54:2117–2125. [PubMed: 15983213]
22. Armarego, WLF.; Perrin, DD. Purification of Laboratory Chemicals. (Butterworth-Heinemann). Vol. 4. 1998.
23. Abedini A, Raleigh DP. Incorporation of pseudoproline derivatives allows the facile synthesis of human IAPP, a highly amyloidogenic and aggregation-prone polypeptide. Org Lett 2005;7:693–696. [PubMed: 15704927]
24. Marek P, Abedini A, Song B, Kanungo M, Johnson M, Gupta R, Zaman W, Wong S, Raleigh D. Aromatic interactions are not required for amyloid fibril formation by islet amyloid polypeptide but do influence the rate of fibril formation and fibril morphology. Biochemistry 2007;46:3255–3261. [PubMed: 17311418]
25. Cort J, Liu Z, Lee G, Harris SM, Prickett KS, Gaeta LS, Andersen NH. Beta-structure in human amylin and two designer beta-peptides: CD and NMR spectroscopic comparisons suggest soluble beta-oligomers and the absence of significant populations of beta-strand dimers. Biochem Biophys Res Commun 1994;204:1088–1095. [PubMed: 7980582]
26. Abedini A, Raleigh DP. The role of His-18 in amyloid formation by human islet amyloid polypeptide. Biochemistry 2005;44:16284–16291. [PubMed: 16331989]
27. Koo BW, Miranker AD. Contribution of the intrinsic disulfide to the assembly mechanism of islet amyloid. Protein Sci 2005;14:231–239. [PubMed: 15576552]
28. Padrick SB, Miranker AD. Islet amyloid polypeptide: identification of long-range contacts and local order on the fibrillogenesis pathway. J Mol Biol 2001;308:783–794. [PubMed: 11350174]

29. Padrick SB, Miranker AD. Islet amyloid: phase partitioning and secondary nucleation are central to the mechanism of fibrillogenesis. Biochemistry 2002;41:4694–4703. [PubMed: 11926832]
30. Abedini A, Raleigh DP. Destabilization of human IAPP amyloid fibrils by proline mutations outside of the putative amyloidogenic domain: is there a critical amyloidogenic domain in human IAPP? J Mol Biol 2006;355:274–281. [PubMed: 16303136]
31. Abedini A, Singh G, Raleigh DP. Recovery and purification of highly aggregation-prone disulfide-containing peptides: application to islet amyloid polypeptide. Anal Biochem 2006;351:181–186. [PubMed: 16406209]
32. Goldsbury C, Green J. Time-lapse atomic force microscopy in the characterization of amyloid-like fibril assembly and oligomeric intermediates. Methods Mol Biol 2005;299:103–128. [PubMed: 15980598]
33. Green JD, Goldsbury C, Kistler J, Cooper GJS, Aebi U. Human amylin oligomer growth and fibril elongation define two distinct phases in amyloid formation. J Biol Chem 2004;279:12206–12212. [PubMed: 14704152]
34. Green J, Goldsbury C, Mini T, Sunderji S, Frey P, Kistler J, Cooper G, Aebi U. Full-length rat amylin forms fibrils following substitution of single residues from human amylin. J Mol Biol 2003;326:1147–1156. [PubMed: 12589759]
35. Kapurniotu A, Bernhagen J, Greenfield N, Al-Abed Y, Teichberg S, Frank RW, Voelter W, Bucala R. Contribution of advanced glycosylation to the amyloidogenicity of islet amyloid polypeptide. Eur J Biochem 1998;251:208–216. [PubMed: 9492286]
36. Jaikaran ETAS, Nilsson MR, Clark A. Pancreatic beta-cell granule peptides form heteromolecular complexes which inhibit islet amyloid polypeptide fibril formation. Biochem J 2004;377:709–716. [PubMed: 14565847]
37. de Koning SBCEJ, Clark A. Effect of pH and insulin on fibrillogenesis of islet amyloid polypeptide in vitro. Biochemistry 1995;34:14588–14593. [PubMed: 7578065]
38. Kudva YC, Mueske C, Butler PC, Eberhardt NL. A novel assay in vitro of human islet amyloid polypeptide amyloidogenesis and effects of insulin secretory vesicle peptides on amyloid formation. Biochem J 1998;331:809–813. [PubMed: 9560308]
39. Bosco DA, Fowler DM, Zhang Q, Nieva J, Powers ET, Wentworth P, Lerner RA, Kelly JW. Elevated levels of oxidized cholesterol metabolites in Lewy body disease brains accelerate alpha-synuclein fibrilization. Nat Chem Biol 2006;2:249–253. [PubMed: 16565714]
40. Luca S, Yau WM, Leapman R, Tycko R. Peptide Conformation and Supramolecular Organization in Amylin Fibrils: Constraints from Solid-State NMR. Biochemistry 2007;46:13505–13522. [PubMed: 17979302]
41. Balasubramaniam A, Renugopalakrishnan V, Stein M, Fischer JE, Chance WT. Syntheses, structures and anorectic effects of human and rat amylin. Peptides 1991;12:919–924. [PubMed: 1800955]
42. Williamson JA, Miranker AD. Direct detection of transient alpha-helical states in islet amyloid polypeptide. Protein Sci 2007;16:110–117. [PubMed: 17123962]
43. Breeze AL, Harvey TS, Bazzo R, Campbell ID. Solution structure of human calcitonin gene-related peptide by 1H NMR and distance geometry with restrained molecular dynamics. Biochemistry 1991;30:575–582. [PubMed: 1988044]
44. Amodeo P, Morelli MA, Motta AC. Multiple conformations and proline cis-trans isomerization in salmon calcitonin: a combined nuclear magnetic resonance, distance geometry, and molecular mechanics study. Biochemistry 1994;33:10754–10762. [PubMed: 8075076]
45. Kayed R, Bernhagen J, Greenfield N, Sweimeh K, Brunner H, Voelter W, Kapurniotu A. Conformational transitions of islet amyloid polypeptide (IAPP) in amyloid formation in vitro. J Mol Biol 1999;287:781–796. [PubMed: 10191146]
46. Powers ET, Powers DL. The kinetics of nucleated polymerizations at high concentrations: amyloid fibril formation near and above the “supercritical concentration”. Biophys J 2006;91:122–132. [PubMed: 16603497]
47. Krampert M, Bernhagen J, Schmucker J, Horn A, Schmauder A, Brunner H, Voelter W, Kapurniotu A. Amyloidogenicity of recombinant human pro-islet amyloid polypeptide (ProIAPP). Chemistry and Biology 2000;7:855–871. [PubMed: 11094339]

48. Pawara AP, DuBaya KF, Zurdoa J, Chitib F, Vendruscoloa M, Dobson CM. Prediction of "Aggregation-prone" and "Aggregation-susceptible" Regions in Proteins Associated with Neurodegenerative Diseases. J Mol Biol 2005;350:379–392. [PubMed: 15925383]

49. Balch WE, Morimoto RI, Dillin A, Kelly JW. Adapting proteostasis for disease intervention. Science 2008;319:916–919. [PubMed: 18276881]

50. Özcan U, Cao Q, Yilmaz E, Lee AH, Iwakoshi NN, Özdelen E, Tuncman G, Gorgun C, Glimcher LH, Hotamisligil G. Endoplasmic reticulum stress links obesity, insulin action, and type 2 diabetes. Science 2004;306:457–461. [PubMed: 15486293]

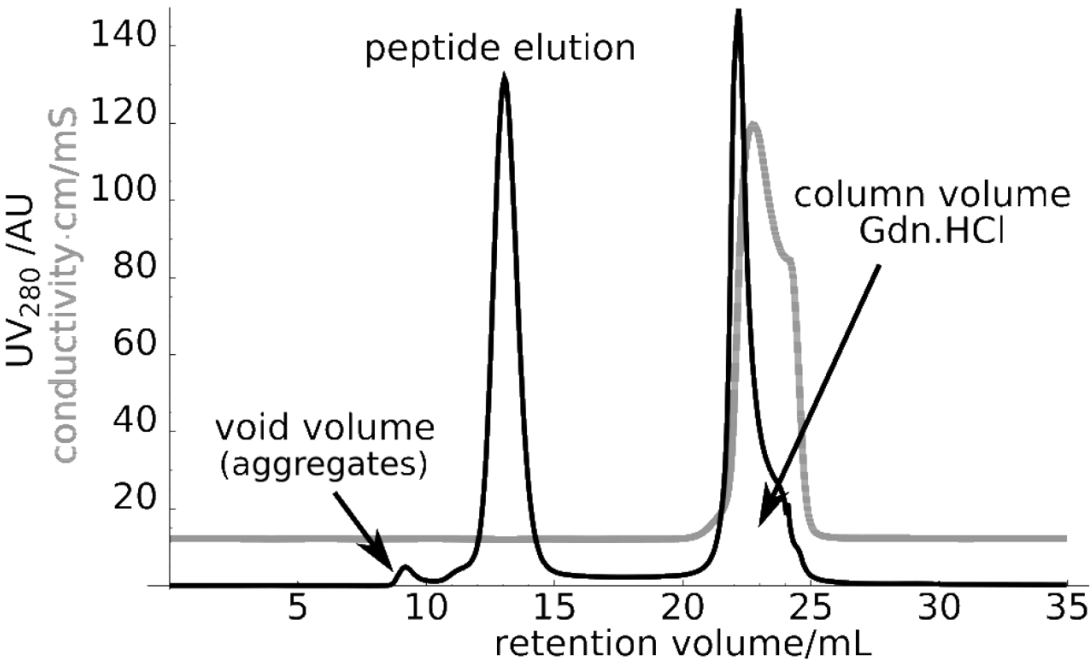

Figure 1.

A typical FPLC size exclusion chromatogram accomplishes buffer exchange and elimination of aggregates prior to experimentation. Absorbance is measured at 280 nm (black trace) and conductivity (grey trace) indicates the passage of guanidinium chloride. The UV peak near the void volume was not always observed and had varying intensities. The elution time shown is representative for amylin; for the longer processing intermediates, the elution times are earlier but still separate from the void volume and consistent between runs.

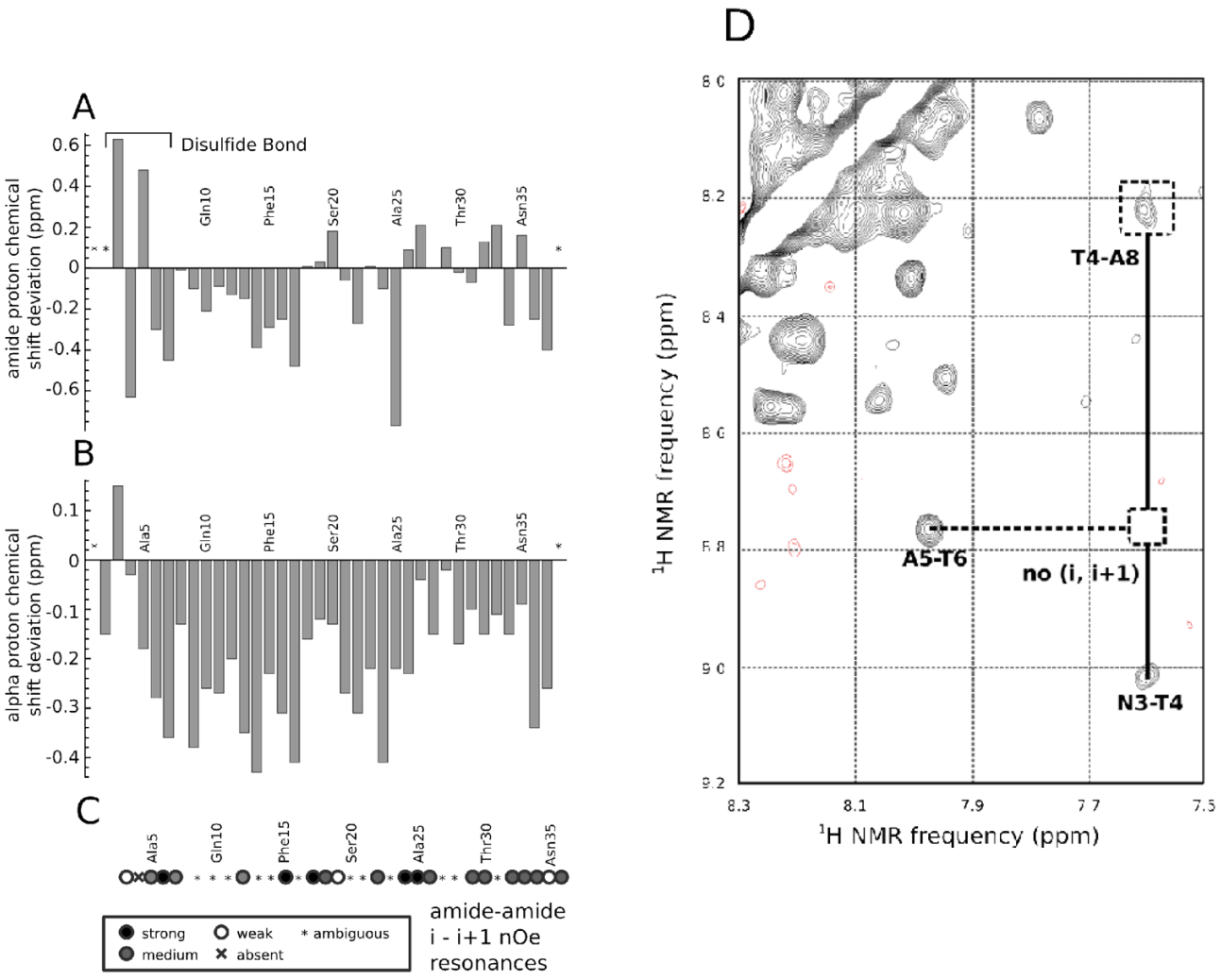

Figure 2.

Amide proton (A) and alpha proton (B) chemical shift deviations in solution phase NMR of amylin with structural features highlighted; asterisks indicate residues whose chemical shifts were indeterminate due to rapidly solvent-exchanging protons. List of NOE resonances between sequential amide protons (C). Black filled circles represent strong (i, i+1) interactions, grey filled circles represent medium-strength interactions, and open circles represent weak interactions. Asterisks indicate resonance pairs where the (i, i+1) interaction is ambiguous due to proximity to the diagonal. The T4-A5 pair lacks an (i, i+1) amide pair. Instead the threonine 4 residue amide proton is proximal to the alanine 8 amide proton (D), suggesting an inversion of amide polarity caused by the presence of the disulfide bond.

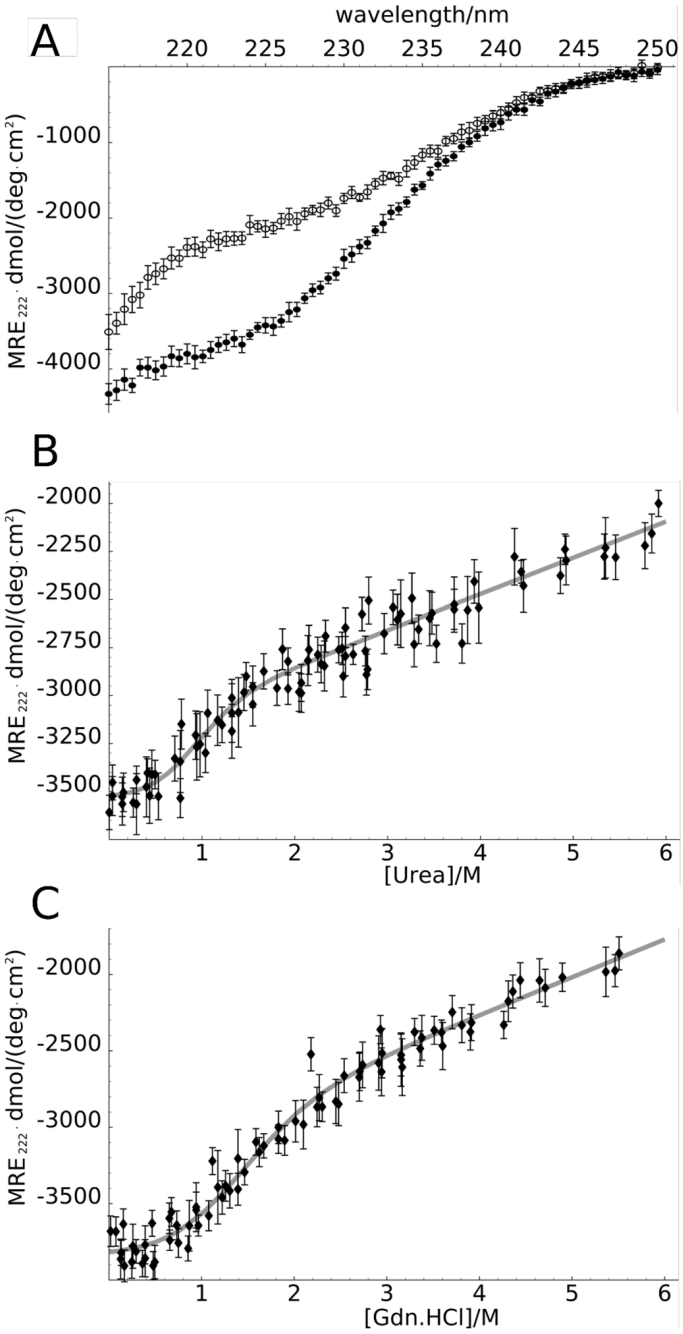

Figure 3.

Denaturant diminishes the amplitude of amylin's ellipticity. The difference in spectra (A) between biomimetic buffer (10 mM P_i, 100 mM NaCl, pH 6.0, filled circles) and denaturing buffer (10 mM P_i, 100 mM NaCl, 4 M GdnHCl, pH 6.0, open circles) suggests the loss of structure under the latter conditions. Urea (B) and guanidine (C) denaturation curves based on ellipticity at 222 nm wavelength. This wavelength exhibits the greatest difference in ellipticity when recorded under biomimetic and denaturing buffer conditions. The folding curves suggest a modestly cooperative folding transition, modeled by the grey curves.

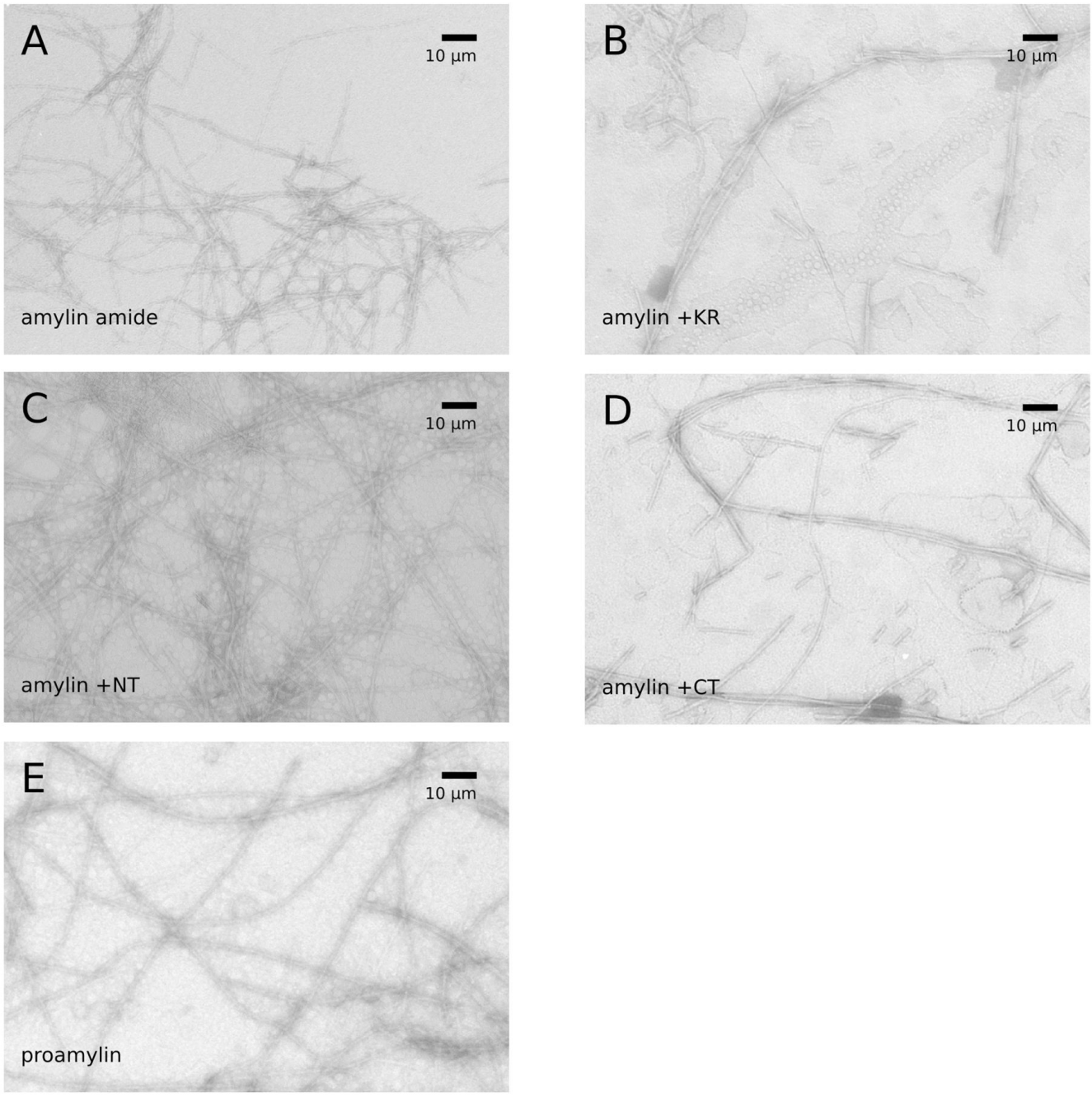

Figure 4.
EM images reveal that amylin (A), amylin+KR (B), amylin+NT (C), amylin+CT (D), and proamylin (E) all form fibrillar aggregates when aggregated at 100 μM overnight. All fibrils were formed by preseeding (1:10) with a quiescently generated, fibrillized sample of the respective peptides at a concentration of 100 μM, except for proamylin, which required agitation to form the seed fibrils.

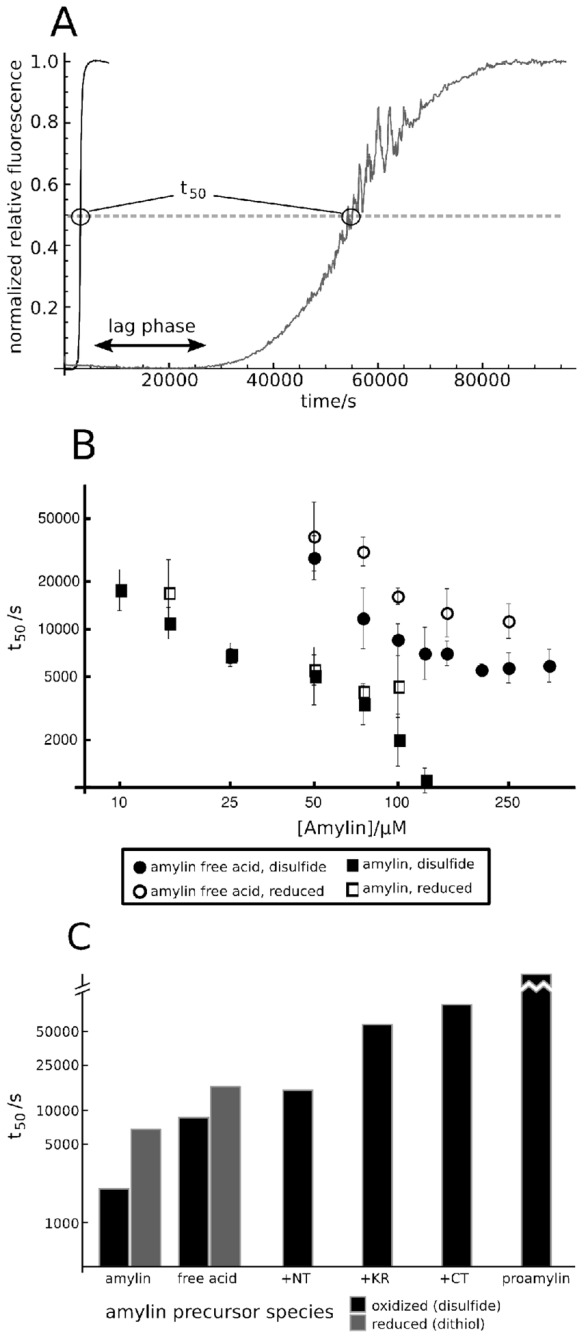

Figure 5.

Representative kinetic curves for amylin at 125 μM (black) and 25 μM (grey), normalized against the 10 highest and 10 lowest consecutive fluorescence points, and demonstrating the t_{50} measurement (A). Further representative curves are presented in the Supporting Information. Kinetics of oxidized (filled, geometric mean of five experiments) and reduced (open, geometric mean of four experiments) amylin free acid (circle) and amylin (square) amyloidogenesis (B). Relative t_{50} kinetics, geometric mean of four (or five for oxidized amylin free acid and amylin) experiments, of oxidized (black) and reduced (grey) amylin and amylin processing intermediates along the processing pathway, all measured at 100 μM (C). Proamylin

did not aggregate quiescently over the course of 6 days in two separate experiments at this concentration.

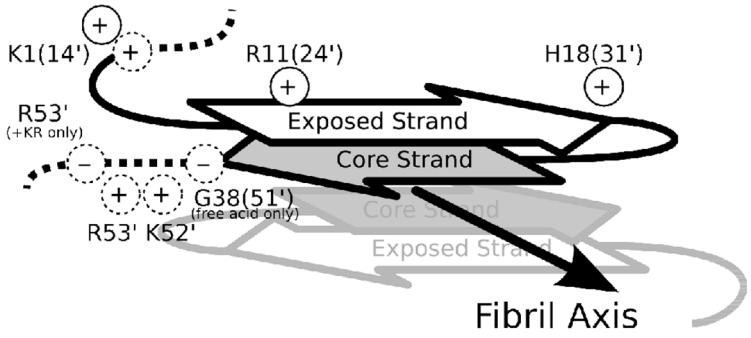

species	net charge	charge flanking core	t_{50} (s)
amylin	+4	0	2.0×10^{3}
amylin free acid	+3	-1	8.6×10^{3}
amylin +NT	+5	0	1.5×10^{4}
amylin +KR	+5	+2-1	5.8×10^{4}
amylin +CT	+5	+2	8.7×10^{4}
proamylin	+6	+2	n.d.

Figure 6.

A schematic diagram of the location of the charges in the fibril, based on the structures reported by Tycko, et al (40). The C-terminus of amylin is buried as a beta strand in the 'core' of the fibril; the N-terminus becomes a half-solvent-exposed beta strand. Charges flanking the C-terminus of amylin in the misprocessed forms may destabilize the fibril by making in-register charges near the buried 'core' strand. t_{50} values are reported as geometric means.

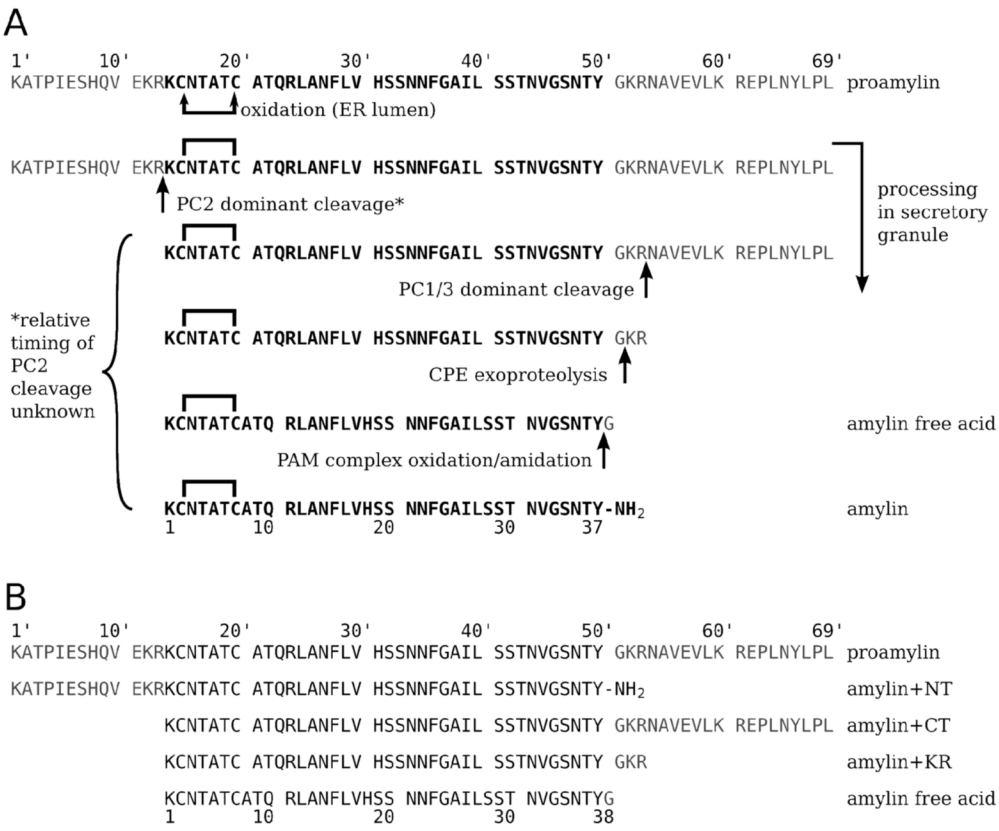

Scheme 1.

(A) proamylin undergoes processing to yield the final, 37-residue, amidated peptide amylin (bold). Amylin processing intermediate sequences are numbered with a (′); amylin sequence numbering is used for the free acid and the amide peptides. The relative timing of PC 2 processing in this scheme is not established, but the steps following PC 1/3 processing must occur in the sequence shown. (B) A list of the peptides studied and nomenclature used in this study.